Fano resonance in the strong-coupling regime

M. Ahsan Zeb
Department of Physics, Quaid-i-Azam University, Islamabad 45320, Pakistan

(Received 28 June 2022; revised 4 October 2022; accepted 6 October 2022; published 18 October 2022)

Fano resonance is a well-celebrated weak-coupling phenomenon whereby a small interaction between a discrete and a continuum of excited states leads to an interference between the respective two transition amplitudes, resulting in an asymmetric line shape in the excitation spectra. We present the strong-coupling phase of the Fano's model where the interaction is localized in a region ξ that is smaller than the collective coupling between the discrete state and the continuum. We explore the behavior of the excitation probability σ as a function of ξ, the ratio of the bare transition amplitudes, and the energy of the discrete state. In the strong-coupling phase, the spectral function of the discrete state splits up and produces up to three complete destructive interferences or zeros of σ along with ultrasharp features. We also find that the discrete state does not have to lie within the continuum to produce the well-known weak-coupling profiles of σ as long as the collective coupling is strong enough. In addition, we consider a broadened state instead of a continuum and present a method that exactly treats such cases by explicitly including the source of the broadening—a weak coupling to the continuum of environment states—in the model.

DOI: 10.1103/PhysRevB.106.155134

I. INTRODUCTION

Fano resonance [1] occurs when a discrete or localized state lies within a continuum of states and weakly interacts with them. It shows up as a characteristic profile in the corresponding scattering cross section, owing to an interference between the two possible transition paths. The phenomenon has been observed in a vast variety of systems [2–8] including atoms [1,9,10], quantum dots [11], semiconductor superlattices [12], optical solitons [13,14], Josephson-junction ladders [15,16], photonic crystal slabs [17], plasmonic nanostructures [18–20], single-electron transistors [21], and nano- and mesoscopic interferometers [22,23]. Some recent reviews on Fano resonance in nanostructures [24], metamaterials [25], and photonic devices [26] sum up the literature beautifully.

Fano introduced his model in 1961 to describe the effect of a weak interaction between two electronic configurations of a He atom [1], a discrete doubly excited state and a continuum of singly excited states, to explain the observed asymmetric line shape in the excitation spectrum [9]. Fano showed that the normalized scattering probability σ is described by a simple yet elegant formula,

$$\sigma = \frac{(q+\epsilon)^2}{1+\epsilon^2}, \tag{1}$$

where ϵ is reduced energy and q is called the asymmetry parameter that determines the line shape. It has been applied to numerous situations ever since but always in the weak-coupling regime, where a single discrete state produces a single resonance.

We find that the Fano's original model also has a strong-coupling regime, where the discrete state splits up to produce two additional resonances that are below and above the original one. This happens when the interaction is localized in a region of the continuum ξ that is smaller than its collective coupling Ω. In the strong-coupling regime, the formula in Eq. (1) remains the same but the behavior of ϵ and q differs qualitatively. ϵ becomes a nonmonotonic function of energy with up to three zeros each leading to a separate resonance, whereas q acquires a strong energy dependence and cannot be taken as a parameter anymore.

Figure 1 illustrates the Fano's model and its two coupling regimes that are distinguished by the nature of its continuum eigenstates $|\Psi_E\rangle$. A discrete state $|\phi\rangle$ and a continuum of states $|\psi_E\rangle$ are coupled via V_E, while we like to study the probability of excitation from a decoupled state $|i\rangle$ [Fig. 1(a)]. The spectral function of $|\phi\rangle$ defined as $\mathcal{A}_\phi = |\langle\phi|\Psi_E\rangle|^2$ is shown on red to yellow (black to white) scale in Figs. 1(b) and 1(c), where it is concentrated around the bare energy of $|\phi\rangle$ in the weak-coupling regime [Fig. 1(b)] but splits up in the strong-coupling regime [Fig. 1(c)].

We see that the terminology here shares the same basic intuition as in the context of various quantum electrodynamic (QED) systems [27], where the weak-coupling means slightly modified bare states around their bare energies while the strong-coupling means emergence of new blue- and redshifted "resonances" (hybrid states called polaritons). Here in the Fano's model the physical quantity that interests us is the excitation probability σ instead of the spectral function of $|\phi\rangle$ (which in some cases can be equivalent, e.g., optical absorption in QED systems [28]) where these resonances exhibit sharp jumps in the scattering phase shift (of size π, as we will see later), so there is a single jump in the weak-coupling regime but additional jumps appear in the strong-coupling regime. There is another resemblance. While in cavity QED, the coupling has to overcome the cavity and emitter losses to

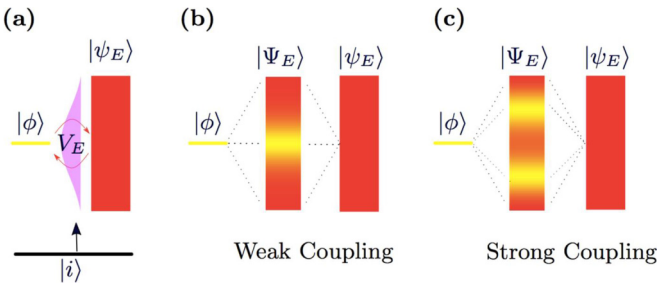

FIG. 1. A depiction of the Fano's model and its two coupling regimes. (a) A discrete state $|\phi\rangle$ interacting with a continuum of states $|\psi_E\rangle$ through V_E that is localized in small region. We like to study its effect on the transitions from another state $|i\rangle$ to the continuum of the stationary states $|\Psi_E\rangle$ created by $|\phi\rangle$ and $|\psi_E\rangle$. [(b) and (c)] The formation of the stationary states $|\Psi_E\rangle$ with the spectral function $\mathcal{A}_\phi$ of $|\phi\rangle$ shown on a red to yellow (black to white) scale, where (b) it is peaked around the bare energy of $|\phi\rangle$ in the weak-coupling regime but (c) splits up to create two peaks in the strong-coupling regime.

enter the strong matter-light coupling regime, it will have to overcome the "width" of the interaction in the present case. Since the losses also introduce a homogeneous broadening to the cavity and emitter states, introducing a "width" in their mutual interaction, they play a similar role.

In fact, the interaction between a discrete state and a *homogeneously* broadened plasmon state has been studied by Giannini *et al.* [18,19] using the Fano's model by pretending that the broadened state acts like a flat continuum of states with its Lorentzian line shape transferred to the interaction *and* the bare transition amplitude of the continuum. Following this work, multiple broadband states of an array of plasmonic metamolecules coupled to a discrete vibrational state have also been treated this way [29]. The method successfully describes the experimental observations [18,19,29] but has never been used to describe the strong-coupling phase of the Fano's model. Besides, it is not suitable for a genuine continuum for which the bare transition matrix element does not usually have the specific energy dependence considered in this method. Considering that a Lorentzian broadening to an otherwise discrete state is caused by a constant interaction with a continuum of "environment" states, we will see that this *open* quantum system can also be dealt with by including such an environment into the model explicitly.

In contrast, Fano's model with a localized interaction can naturally appear in a *closed* quantum system. For example, thermodynamically large numbers of *inhomogeneously* broadened emitters collectively coupled to a cavity mode can be swapped perfectly legitimately with a flat continuum with the original emitters' density of states (DOS) profile transferred to the interaction with the cavity mode [28] (details later). Assuming a Gaussian distribution of emitter energies that is suitable for the inhomogeneous broadening arising from random energetic disorder, and has a relatively localized profile as well, we have recently demonstrated that both coupling regimes of the Fano's model are easily accessible [28].

As far as the scattering probability is concerned, the mathematical structure of the model with a genuine continuum is different from that with a broadened state due to a different energy dependence of their bare transition amplitudes. However, the physical meaning of the eigenstates of the two models distinguishes them at a more fundamental level. The eigenstates continuum is formed by a continuum of system states in one case but a continuum of environment states in the other (details later), which requires a projection back onto the system Hilbert space. This restores the relative importance of the broadened state making the "eigenstates" of the system more hybrid (but still broadened of course) in contrast to the other case where the system continuum destroys the hybrid nature of its eigenstates at moderate interaction widths. This point has also been explained in a different manner elsewhere [28] by discretizing the continuum in an equispaced grid with the separation between two states playing the role of the homogeneous broadening of the states.

Here we first show how an important class of physical systems—cavity QED with energetic disorder—is described by the Fano's model with a localized interaction, thus providing us with a strong motivation to study both its phases. We will then consider the generic Fano's model with a tunable interaction and explore its behavior as we move from the weak- to the strong-coupling regime. The discrete state splits up in the strong-coupling regime and creates destructive interference at multiple energies where σ can vanish completely. We also find that if the coupling is strong enough, then the weak-coupling profiles of σ [24] can be mimicked even when the discrete state lies well outside the continuum. Considering that a localized interaction is also relevant in case of a broadened state [18] instead of a genuine continuum, for completeness, we will describe a method to deal with broadened states in lossy systems that explicitly considers the source of the broadening—a weak coupling to a continuum of environment states—to make it a closed system and compute the desired quantities by diagonalizing this closed system.

Section II shows the emergence of Fano's model from the Tavis-Cummings (TC) model [30,31] that describes the collective interaction of a large ensemble of energetically disordered emitters to a cavity mode. In Sec. III, we give a brief overview of the Fano's seminal work [1] and describe the condition for the strong-coupling regime. Our calculations and results for a tuneable Gaussian interaction are presented in Sec. IV, where Sec. IV A gives the expressions for the Fano's parameters, Sec. IV B relates them to the weak-coupling case, Sec. IV C compares the Fano profile in the two-coupling regime, and Sec. IV D gives the phase diagram of the model when the discrete state coincides with the interaction maximum. The effect of a finite detuning is discussed in Sec. IV E, a special case of which with the discrete state lying outside the continuum is presented in Sec. IV F. Finally, Sec. V presents our approach to deal with a system with broadened states.

II. MOTIVATION: DISORDERED TAVIS-CUMMINGS MODEL

An important physical system where the interaction between a discrete state and a continuum of states turns out to be strongly localized is a microcavity with an energetically disordered ensemble of emitters. While the single photon state of the microcavity is a discrete state, we find that the emitters' states can be transformed to a nondegenerate continuum of

bright (superradiant) states, with their interaction to the cavity state determined by the emitters' DOS, which is usually a localized Gaussian distribution [28]. This system can realize the strong-coupling phase of the Fano's model where the eigenstates of the system become hybrid light-matter excitations called polaritons at low energetic disorder [28]. Such hybrid matter-light systems are important due to their technological prospects [32–36] and have been extensively studied [37–43].

Consider $\mathcal{N}$ emitters (two level systems) with transition energies $\{E_{x,n}\}$ randomly chosen from a probability distribution P_E. If these emitters couple to a common cavity mode, then the system is described by the TC model [30,31] that, in the single excitation space (one cavity photon or a single excited emitter), can be written as

$$H_{\rm TC} = E_c\,|1_P\rangle\langle 1_P| + \sum_{n=1}^{\mathcal{N}} E_{x,n}\,|\uparrow_n\rangle\langle\uparrow_n| + \frac{\Omega_R}{\sqrt{\mathcal{N}}}\{|1_P\rangle\langle\uparrow_n| + |\uparrow_n\rangle\langle 1_P|\}, \tag{2}$$

where $|1_P\rangle$ is the cavity state with a photon at energy E_c, $|\uparrow_n\rangle$ is the state with nth emitter excited, and Ω_R is the collective coupling of the emitters. The effects of the inhomogeneous broadening on the optical absorption of the TC model has been studied before by considering the continuous limit of the model and treating the homogeneous broadening of the cavity and emitter states as imaginary components of their bare energies as in the Green's function method [44–46]. Here we focus on the emergence of the Fano's model as a result of the inhomogeneous broadening [28]. If $E_{x,n} = E_0$, $\forall n \in [1, \mathcal{N}]$, then the bright and dark states [47] given by

$$|B\rangle = \frac{1}{\sqrt{\mathcal{N}}}\sum_{n=1}^{\mathcal{N}} |\uparrow_n\rangle\,, \tag{3}$$

$$|d_k\rangle = \frac{1}{\sqrt{\mathcal{N}}}\sum_{n=1}^{\mathcal{N}} e^{ikn2\pi/\mathcal{N}}\,|\uparrow_n\rangle\,, \tag{4}$$

where $k \in [1, \mathcal{N}-1]$, block diagonalize $H_{\rm TC}$. That is $H_{\rm TC} = H_{{\rm TC},B} + H_{{\rm TC},D}$ where

$$H_{{\rm TC},B} = E_c\,|1_P\rangle\langle 1_P| + E_0\,|B\rangle\langle B| + \Omega_R\{|1_P\rangle\langle B| + |B\rangle\langle 1_P|\} \tag{5}$$

is the bright sector of the model that is decoupled from the dark sector given by

$$H_{{\rm TC},D} = E_0\sum_{k=1}^{\mathcal{N}-1} |d_k\rangle\langle d_k|\,. \tag{6}$$

This is an important transformation as it reduces the problem size from $\mathcal{N}+1$ to only 2, along with a set of $\mathcal{N}-1$ dark eigenstates $\{|d_k\rangle\}$ at bare emitter energy E_0. The same transformation fails to decouple the bright and dark sectors if the emitters' transition energies are different.

Interestingly, however, if we make subsets of degenerate emitters and apply the same transformation to individual degenerate energy levels, then we can still decouple the bright and dark sectors to obtain one bright state per energy level [28], as follows. Suppose there are a total of N energy levels with mth level at energy E_m being K_m-fold degenerate. We can relabel the emitters according to these levels so that if $E_{x,n} = E_m$ for emitter n, $|\uparrow_n\rangle \to |\uparrow_{m,j}\rangle$ with $j \in [1, K_m]$. Using the above recipe, the *set of bright states* we obtain is

$$|B_m\rangle = \frac{1}{\sqrt{K_m}}\sum_{j=1}^{K_m-1} |\uparrow_{m,j}\rangle\,, \tag{7}$$

where $m \in [1, N]$. Focusing on the bright sector $H_{{\rm TC},B}$ in this case, we thus have

$$H_{{\rm TC},B} = E_c\,|1_P\rangle\langle 1_P| + \sum_{m=1}^{N} E_m\,|B_m\rangle\langle B_m| + V_m\{|1_P\rangle\langle B_m| + |B_m\rangle\langle 1_P|\}, \tag{8}$$

where $V_m = \Omega_R\sqrt{K_m/\mathcal{N}}$. At $\mathcal{N}\to\infty$, the emitters' DOS becomes continuous so $N\to\infty$ and we can take the continuous limit of $H_{{\rm TC},B}$ above to obtain

$$H_{{\rm TC},B} = E_c\,|1_P\rangle\langle 1_P| + \int dE\{|B_E\rangle\langle B_E| + V_E(|1_P\rangle\langle B_E| + |B_E\rangle\langle 1_P|)\}, \tag{9}$$

where $V_E = \Omega_R\sqrt{P_E}$ and the bright states $|B_E\rangle$ are now normalized per unit energy and represent a flat continuum of states. Combined with the ground state of the emitter-cavity system, $|{\rm vac}\rangle$, which has no cavity photon or molecular excitation, the state $|1_P\rangle$ and the continuum $|B_E\rangle$, realize the Fano's model [1] illustrated in Fig. 1(a), with the correspondence $|{\rm vac}\rangle \leftrightarrow |i\rangle$, $|1_P\rangle \leftrightarrow |\phi\rangle$, and $|B_E\rangle \leftrightarrow |\psi_E\rangle$.

We have studied both the weak- and the strong-coupling phases [Figs. 1(b) and 1(c)] of the model in Eq. (9) in the context of organic microcavities in Ref. [28], where the most relevant excitation spectrum that is usually measured in the experiments is the optical absorption. The response to inelastic electron scattering can also be interesting in some cases. Since different excitation processes have different bare transition amplitudes for the discrete and continuum states, the form of $q = q_E$ varies for different physical spectra. As the Fano's model is very versatile and often applied to a variety of physical systems with a range of bare transition amplitudes, the model has to be studied in its full parameter space. This is the main goal of this article. We will henceforth consider the generic Fano's model and explore its parameter space to study its behavior without making any assumptions on the underlying physical system that it describes.

III. FANO'S MODEL

Consider the model illustrated in Fig. 1. We have a discrete state $|\phi\rangle$ at energy E_ϕ and a continuum of states $\{|\psi_E\rangle\}$ at energies $\{E\}$ with a coupling V_E between them. There is another low-energy discrete state $|i\rangle$ and our main goal is to calculate the effect of the interaction V_E on the probability with which the system can be excited from this state. Fano solved this model [1] to explain the asymmetric line shape of a peak in the excitation spectra of He atoms observed in the inelastic scattering of electrons. Let us briefly review the solution of this model.

The Hamiltonian of the system is given by

$$H = E_\phi |\phi\rangle\langle\phi| + \int dE' \{|\psi_{E'}\rangle\langle\psi_{E'}| + V_{E'}(|\phi\rangle\langle\psi_{E'}| + |\psi_{E'}\rangle\langle\phi|)\}, \quad (10)$$

If $V_E \neq 0$, $|\phi\rangle$ and $\{|\psi_E\rangle\}$ are not the eigenstates of the system. The eigenstates $\{|\Psi_E\rangle\}$ of the above Hamiltonian are calculated by Fano [1] and can be written as

$$|\Psi_E\rangle = \frac{\sin\Delta}{\pi V_E}|\Phi\rangle - \cos\Delta\,|\psi_E\rangle, \quad (11)$$

where

$$|\Phi\rangle = |\phi\rangle + \mathcal{f}\frac{V_{E'}}{E-E'}|\psi_{E'}\rangle\,dE', \quad (12)$$

$$\Delta = -\arctan\left[\frac{\pi|V_E|^2}{E-E_\phi-F_E}\right], \quad (13)$$

$$F_E = \mathcal{f}\frac{|V_{E'}|^2}{E-E'}dE', \quad (14)$$

δ is the Dirac δ function, and $\mathcal{f}$ evaluates the (Cauchy) principal value of the integral.

Assume that there is some mechanism that can excite the system from $|i\rangle$ to $|\phi\rangle$ and $\{|\psi_E\rangle\}$, and hence $\{|\Psi_E\rangle\}$. The excitation probability will depend on the squared matrix element $|M_E|^2$ of the corresponding transition operator $\hat{T}$ between the initial and the final state. M_E can be written as [1]

$$M_E \equiv \langle i|\hat{T}|\Psi_E\rangle, = \frac{1}{\pi V_E}\langle i|\hat{T}|\Phi\rangle\sin\Delta - \langle i|\hat{T}|\psi_E\rangle\cos\Delta. \quad (15)$$

Since Δ is an odd function of $E - E_\phi - F_E$ [Eq. (13)], the sine and cosine terms in Eq. (15) will interfere constructively on one side of the resonance at $E = E_\phi + F_E$ but destructively on its other side. Δ sharply changes around this resonance resulting in a sharp dip and a peak structure in the excitation spectrum. This is called Fano resonance after Ugo Fano who explained it decades ago, as discussed below.

The transition operator $\hat{T}$ must couple the initial state $|i\rangle$ to, at least, the continuum $\{\psi_E\}$. That is, we must have $|\langle i|\hat{T}|\psi_E\rangle| > 0$ for the states $|\psi_E\rangle$ around the resonance so that the interference between sine and cosine terms in Eq. (15) can occur. The normalized transition probability σ can be written in terms of a reduced energy ϵ and an asymmetry "parameter" q, as [1]

$$\sigma = \frac{|\langle i|\hat{T}|\Psi_E\rangle|^2}{|\langle i|\hat{T}|\psi_E\rangle|^2}, = \frac{(q+\epsilon)^2}{1+\epsilon^2}, \quad (16)$$

where

$$\epsilon = \frac{E-E_\phi-F_E}{\pi|V_E|^2}, \quad (17)$$

$$q = \frac{1}{\pi V_E}\frac{\langle i|\hat{T}|\Phi\rangle}{\langle i|\hat{T}|\psi_E\rangle}. \quad (18)$$

Equation (16) is the famous Fano formula [also given in Eq. (1)]. If the interaction is weak, then $E - E_\phi - F_E = 0$ has a single root where the phase Δ in Eq. (13) jumps between $\pm\pi/2$ and a resonance occurs, so ϵ in Eq. (17) is a monotonic function of E. This is the case Fano originally considered. However, these results are valid for any interaction V_E for the eigenstates $\{|\Psi_E\rangle\}$ lying within the original continuum, which also includes a "strong-coupling" regime that is qualitatively different from the above weak-coupling regime. In the strong-coupling regime, ϵ becomes a nonmonotonic function as $E - E_\phi - F_E = 0$ is satisfied at multiple energies with corresponding jumps in Δ indicating resonances.

σ is the physical quantity that is measured in the experiments. Depending on exactly what spectrum we like to study in a particular physical system, the ratio γ of the bare transition amplitudes of the discrete state and the continuum for the relevant processes determines q, which, along with ϵ, in turn determines the corresponding excitation spectrum σ. So, the analysis presented in this paper is general and can be applied to a given case by selecting appropriate value of γ, as will be discussed later.

A. Strong- and weak-coupling regimes

It is simple to understand that if the collective coupling Ω defined as

$$\Omega^2 \equiv \int |V_E|^2 dE, \quad (19)$$

is much larger than the bandwidth W of the continuum, i.e., $\Omega \gg W$, the band will act as a highly degenerate level and we will get two discrete eigenstates around the continuum (with an effective 2×2 description in terms of the discrete state $|\phi\rangle$ and the symmetric superposition of the continuum states $\int dE'\,|\psi_{E'}\rangle/\sqrt{W}$).

However, there is another interesting strong-coupling regime. If the coupling V_E is localized in a narrow region ξ of the continuum such that

$$\xi < \Omega \ll W, \quad (20)$$

then the discrete level $|\phi\rangle$ still splits but remains inside the continuum. We can confirm this from appearance of new resonances, discontinuities or jumps in the phase Δ. The spectral function $\mathcal{A}_\phi$ of the discrete state $|\phi\rangle$ splits into multiple peaks around these new resonances under such a condition.

If the condition in Eq. (20) does not hold for any region of the continuum, then we are in the weak-coupling regime where the phase Δ jumps only once. The extreme case, $\xi \gg \Omega$, describes the case originally considered by Fano, where Δ jumps almost at the bare energy E_ϕ of the discrete state $|\phi\rangle$ with $\mathcal{A}_\phi$ localized around it. In this case, ϵ is a linear function of E and q can be taken as an energy-independent parameter, as will later be shown in this article.

In this work, we will assume that $\Omega \ll W$ and all eigenstates lie within the continuum so that all the above results hold. We will take a tuneable interaction to explore the behavior of the model as we go from weak- to the strong-coupling regime.

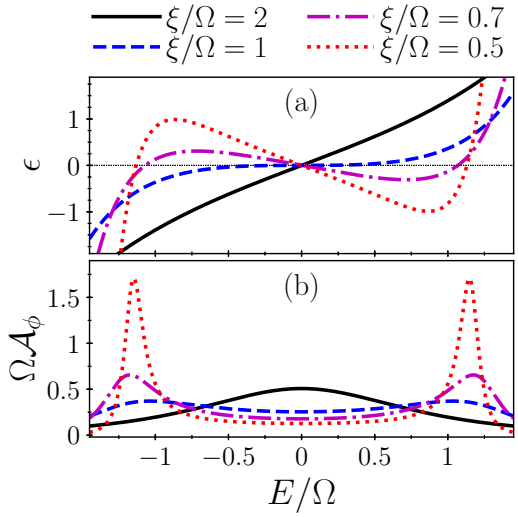

FIG. 2. The weak- and strong-coupling regimes. (a) Reduced energy ϵ changes from a monotonic to a nonmonotonic function of energy E along with appearance of new resonances as we move from the weak ($\xi/\Omega \geqslant 1$) to the strong-coupling regime ($\xi/\Omega < 1$). (b) The spectral function of the discrete state $\mathcal{A}_\phi$ splits up as we enter the strong-coupling regime.

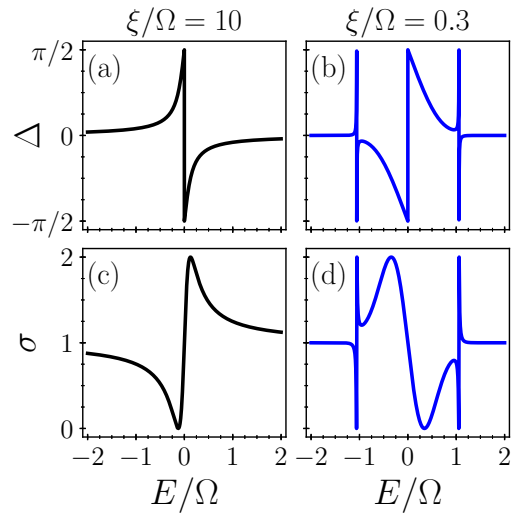

FIG. 3. Fano resonance in the two coupling regimes at $\xi/\Omega = 10, 0.2$ and $E_\phi = 0$ assuming $q = 1$. In the weak-coupling regime ($\xi/\Omega = 10$), there is only a single abrupt jump (a) in the phase angle Δ and hence a single Fano resonance exhibited by (b) the normalized excitation probability σ. In the strong-coupling regime ($\xi/\Omega = 0.3$), on the other hand, we see that (c) Δ jumps at three locations and so (d) σ develops three Fano resonances.

IV. TRANSITION BETWEEN THE WEAK- AND THE STRONG-COUPLING REGIMES

Let us consider a Gaussian interaction that is localized around $E = 0$, given by

$$V_E^2 = \Omega^2 \frac{1}{\sqrt{2\pi\xi^2}} e^{-E^2/2\xi^2}, \tag{21}$$

so that we can tune its width ξ to move between the weak- and the strong-coupling regimes. Using Eq. (21) and Eq. (14), and noting that the contribution of the off-resonant states exponentially decay, we can integrate over the whole interval $E \in [-\infty, \infty]$ to obtain

$$F_E = \frac{\sqrt{2}\Omega^2}{\xi} D(E/\sqrt{2}\xi), \tag{22}$$

where D is the Dawson function given by $D(x) = \sqrt{\pi} e^{-x^2} \mathrm{erfi}(x)/2$ and erfi is the imaginary error function. Using Eq. (22) and Eq. (21), ϵ in Eq. (17) can be written as

$$\epsilon = \sqrt{\frac{2}{\pi}} \frac{\xi}{\Omega^2} e^{E^2/2\xi^2} (E - E_\phi) - \mathrm{erfi}(E/\sqrt{2}\xi). \tag{23}$$

Figure 2(a) shows ϵ as a function of E/Ω at $\xi/\Omega = 2, 1, 0.7, 0.5$ that show transition from weak to the strong coupling as ξ/Ω drops below 1. At $\xi/\Omega \gg 1$, ϵ has a single zero at $E = 0$ but it obtains a curvature as $\xi/\Omega \to 1$ and at $\xi/\Omega = 1$ this zero becomes an inflection point. At $\xi/\Omega < 1$, ϵ acquires two more zeros around $E = 0$ indicating the appearance of new resonances there.

The spectral function $\mathcal{A}_\phi$ is given by

$$\mathcal{A}_\phi \equiv |\langle\phi|\Psi_E\rangle|^2 = \frac{V_E^2}{(E - E_\phi - F_E)^2 + \pi^2 V_E^4}, \\ = \frac{1}{\pi^2 V_E^2} \frac{1}{1 + \epsilon^2}, \tag{24}$$

where Eqs. (12), (13), and (17) have been used. Figure 2(b) shows $\mathcal{A}_\phi$ as a function of E/Ω at the same values of ξ/Ω as in Fig. 2(a). We see that the appearance of new zeros of ϵ accompanies the usual signature of the strong coupling: $\mathcal{A}_\phi$ splitting up into two new peaks. There is in fact an exponentially small residual peak of $\mathcal{A}_\phi$ at $E = 0$ that is invisible in the figure. It is suppressed due to a factor of ξ arising from the prefactor $1/V_E^2$ in Eq. (24). We find that going from the weak to the strong-coupling regime, $\mathcal{A}_\phi$ develops two new peaks at $\xi/\Omega > 1$ before the weak-coupling resonance actually splits at $\xi/\Omega = 1$, as exhibited by the emergence of new zeros of ϵ (or corresponding jumps in the phase angle Δ, shown below). We ignore this detail in this work.

Establishing the above distinction between the two coupling regimes, we can now see how the Fano resonance compares for them. As we will see later, despite the fact that the asymmetry parameter q in Eq. (18) can be assumed constant over the relevant energy window in the weak-coupling regime, it is a function of E in general. But, to focus on the effect of nonmonotonic nature of ϵ, let us ignore the energy dependence of q for the time being. We will see how it affects the resonance later.

Figure 3 shows the phase angle Δ and normalized excitation probability σ at $\xi/\Omega = 10, 0.3$ and $q = 1$. We see that while there is a single jump of size π in the phase Δ in the weak-coupling regime [Fig. 3(a), $\xi/\Omega = 10$], there are three such jumps in the strong-coupling regime [Fig. 3(b),

$\xi/\Omega = 0.3$], with the two new resonances being ultrasharp. This is reflected in the corresponding excitation probabilities σ, shown in Figs. 3(c) and 3(d), where we see one and three Fano resonances. In the context of the weak-coupling case [1], the two new resonances in the strong-coupling regime have the asymmetry parameter $q > 0$ but it seems as if the sign of q for the middle resonance is flipped, exchanging the dip and peak locations. This means that the constructive and destructive interference have switched their places around the resonance. Looking at the evolution of the Fano resonance from weak- to the strong-coupling regimes, we find that this is due to the fact that the two new resonances are evolved from the dip and the peak of the original one and the middle resonance simply has to flip to smoothly connect the two.

In Figs. 3(c) and 3(d), we assumed that q in Eq. (18) is a constant parameter. However, since this approximation holds only in special circumstances for realistic situations, let us now see how the energy dependence of q changes this picture.

A. Energy dependence of q and Fano profile

The energy dependence of q cannot be ignored in general. In this section, we will explore how σ behaves when full energy-dependent q is considered.

Let us take

$$\alpha = \langle i|\hat{T}|\phi\rangle\,, \tag{25}$$

$$\beta = \langle i|\hat{T}|\psi_E\rangle\,, \tag{26}$$

and assume that β is independent of E in the relevant energy window. This is a fair assumption for genuine continua [1] in contrast to a broadened state described as a continuum, where β has to be strongly energy dependent [18] to give the correct excitation spectrum, as we have already discussed in the introduction section. We can now evaluate Eq. (18) to obtain

$$q\pi V_E = \frac{\alpha}{\beta} + \frac{\Omega}{\sqrt[4]{2\pi\xi^2}}\int \frac{e^{-E'^2/4\xi^2}}{E-E'}dE', \tag{27}$$

$$= \frac{\alpha}{\beta} + \frac{\Omega}{\sqrt[4]{2\pi\xi^2}}\pi e^{-E^2/4\xi^2}\mathrm{erfi}(E/2\xi), \tag{28}$$

$$q = \gamma\sqrt{\frac{\xi}{\Omega}}\sqrt[4]{\frac{2}{\pi^3}}e^{E^2/4\xi^2} + \mathrm{erfi}(E/2\xi), \tag{29}$$

where $\gamma = \alpha/\beta\sqrt{\Omega}$ is a dimensionless parameter. Taking Ω as the energy scale, we now have two independent parameters of the model, γ and ξ, that control the scattering probability σ.

For hybrid light-matter systems described in Sec. II, we have the following correspondance $|1_P\rangle \leftrightarrow |\phi\rangle$, $|B_E\rangle \leftrightarrow |\psi_E\rangle$, and can be interested in scattering of two types of excitations, photon and electrons [28]. The first is optical absorption where we have $\alpha \neq 0, \beta = 0$ so $\gamma = \infty$ (we can avoid the normalization with $\beta = 0$, however), whereas in the second case, it is the inelastic scattering of electrons for which $\alpha = 0, \beta \neq 0$ so $\gamma = 0$ [28]. The inelastic electron scattering can be relevant when the emitters are in the gas phase. Here we explore the behavior of σ at general γ to study the behavior of the model without limiting ourselves to a particular physical system or a particular scattering mechanism.

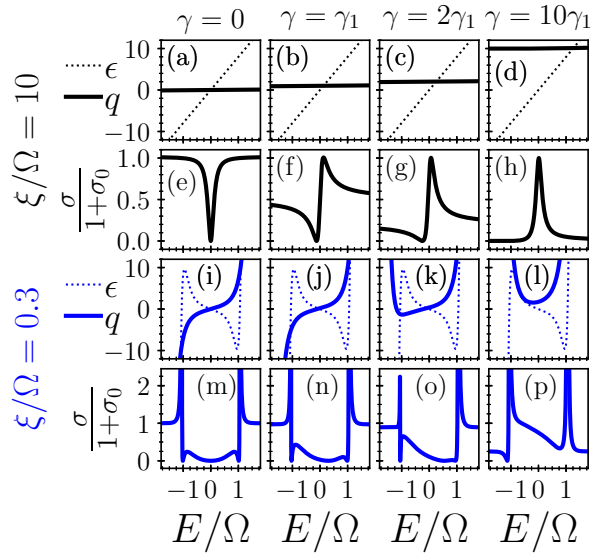

FIG. 4. Comparison between *exact* weak- and strong-coupling results at $\xi/\Omega = 10, 0.3$ and $\gamma/\gamma_1 = 0, 1, 2, 10$, where $\gamma_1 = \sqrt{1/10}(\pi^3/2)^{1/4}$ sets $\gamma/\gamma_1 \simeq q$ in the weak-coupling regime. Panels (a)–(d) and (i)–(l) show q, ϵ. We see that in (a)–(d) q is practically a constant and ϵ has a linear energy dependence, while both are strongly energy dependent in (i)–(l). The corresponding σ is shown in (e)–(h) (that shows well-known weak-coupling profiles) and (m)–(p), respectively. We see multiple ultrasharp Fano resonances in the latter case.

B. q and ϵ in the weak-coupling regime

We find that at $\xi/\Omega \gg 1$, i.e., in the weak-coupling regime, we can take $E/\xi \ll 1$ and expand q to $\mathcal{O}(E/\xi)$ using $\mathrm{erfi}(x) \simeq 2x/\sqrt{\pi}$ at $x \ll 1$. We obtain

$$q \simeq \sqrt{\frac{\xi}{\Omega}}\left(\frac{2}{\pi^3}\right)^{1/4}\gamma + \frac{1}{\sqrt{\pi}\xi}E, \tag{30}$$

$$\approx \sqrt{\frac{\xi}{\Omega}}\left(\frac{2}{\pi^3}\right)^{1/4}\gamma, \tag{31}$$

as the factor $1/\xi$ in the second term makes it too small to be significant at the relevant energies. q can thus be taken as an energy-independent parameter in this case. Similarly, we can reduce Eq. (23) to

$$\epsilon \simeq \sqrt{\frac{2}{\pi}}\frac{\xi}{\Omega^2}(E - E_\phi), \tag{32}$$

where $F_E \simeq (\Omega/\xi)^2 E$ can be ignored as it only produces a very small shift at $\xi \gg \Omega$. Equations (31) and (32) show that, as expected for the weak-coupling regime, q, ϵ can be taken as parameters to describe the Fano resonance.

C. Fano profile

Considering the energy dependence of q as well, we now present the exact results for the line shape or profile in the two coupling regimes. Figure 4 shows $\epsilon, q, \sigma/(1+\sigma_0)$ at $\xi/\Omega = 10, 0.3$ and $\gamma/\gamma_1 = 0, 1, 2, 10$, where σ_0 is the value of σ at $E = 0$ and $\gamma_1 = \sqrt{1/10}(\pi^3/2)^{1/4}$ is chosen to set $\gamma/\gamma_1 \approx q$ at $\xi/\Omega = 10$. ξ changes along the rows while γ

changes along the columns, so the first two rows, Figs. 4(a)–4(h), show the weak-coupling case while the other two rows, Figs. 4(i)–4(p), contain the strong-coupling case. Since ϵ does not depend on γ, Figs. 4(a)–4(d) or Figs. 4(i)–4(l) show the same ϵ as dotted lines. We clearly see that the energy dependence of q in Figs. 4(a)–4(d) is simply unnoticeable and $q \approx \gamma/\gamma_1$. The corresponding evolution of the Fano profile in Figs. 4(e)–4(h) is well known [24]. σ has a dip reaching zero at $\gamma = 0$, a characteristic feature of the Fano resonance arising from complete destructive interference between the transition paths/amplitudes to the modified discrete state $|\Phi\rangle$ and the continuum $\{|\psi_E\rangle\}$. As γ increases above zero, this zero (at $\epsilon = -q$) moves to lower E and a peak (at $\epsilon = 1/q$) develops alongside the dip [Figs. 4(f) and 4(g)], which eventually becomes the dominant feature at $\gamma \gg 1$, as shown in Fig. 4(h).

In the strong-coupling regime, the behavior of q, ϵ, σ is very different. In Figs. 4(i)–4(l), we see that q has a strong energy dependence, which, combined with that of ϵ, produce a much richer picture. We see that at $\gamma = 0$, where q is antisymmetric, σ is symmetric about $E = 0$ [Fig. 4(m)] with three zeros exhibiting complete destructive interference. As γ increases, this symmetry is lost and the central zero moves toward the positive root [Figs. 4(n) and 4(o)]. A further increase in γ merges these zeros and then eliminates them leaving only a partial destructive interference [Fig. 4(p)]. The profile at the other dip (zero of σ) flips during this evolution, i.e., the dip and the peak exchange sides as can be seen here while going from Fig. 4(o) to Fig. 4(p). These results can be summarized in a phase diagram in γ-ξ plane as follows.

D. Phase diagram in γ-ξ plane

On the γ-ξ plane, $\xi/\Omega = 1$ separates the weak- and the strong-coupling regions. The weak-coupling case, $\xi/\Omega > 1$, has a simple behavior. There is always a single zero of ϵ and a single zero of σ. An increase (decrease) of γ away from $\gamma = 0$ produces a peak at positive (negative) energies. However, the strong-coupling region $\xi/\Omega < 1$ is much more interesting. We will divide the phase space depending on two interesting features as follows.

1. Zeros of σ

The scattering probability σ can completely vanish owing to a complete destructive interference, which is a zero of σ at the relevant energy. At $\xi/\Omega < 1$ (and $E_\phi = 0$), there are always three zeros of ϵ and, depending on γ and ξ, one or three zeros of σ. In Fig. 5, the region with one zero is white, whereas the region with three zeros is shaded. Their boundary is shown as a dotted line labeled as γ_z, so $|\gamma_z|$ is the value of $|\gamma|$ above which σ has one zero. We see that $|\gamma_z|$ decreases as ξ/Ω increases. By expanding $q + \epsilon = 0$ at $\gamma = 0$ at small E, it is simple to see (Appendix A 1) that $|\gamma_z| \to 0$ at $\xi/\Omega \to \sqrt{1 - 1/\sqrt{2}}$ when a zero of σ at $E \neq 0$ approaches its zero at $E = 0$.

2. Profile flips

The behavior of the Fano profile is well known in the weak-coupling regime where it flips around the resonance at $\epsilon = 0$ as q is varied across zero, say, $-1 \to +1$, because the constructive and destructive interference exchange places around the resonance. Similar behavior can also be seen for the resonances in the strong-coupling regime. As γ is changed, a zero of q crosses a zero of ϵ (the resonance location) at some specific value $\gamma = \gamma_f$, where the dip and peak structures of σ around the corresponding resonance switch sides. Let us see how γ_f depends on ξ. We can numerically calculate the nonzero roots of $\epsilon = 0$ and then use that to calculate the value of γ at which $q = 0$ is also satisfied. Using Eq. (29), we can thus write

$$\gamma_f = \sqrt{\frac{\Omega}{\xi}} \sqrt[4]{\frac{\pi^3}{2}} e^{-E_0^2/4\xi^2} \operatorname{erfi}(E_0/2\xi), \tag{33}$$

where E_0 is the root of $\epsilon = 0$ where this flip occurs. In Fig. 5, γ_f is shown on the phase diagram as a dashed line. We can see that as $\xi/\Omega \to 1$, $E_0 \to 0$ and $\operatorname{erfi}(E_0/2\xi) \sim E_0$ so $\gamma_f \to 0$ as well. This is expected at $\xi/\Omega \gg 1$ but it is interesting to note that it applies to the whole weak-coupling regime $\xi/\Omega \geqslant 1$.

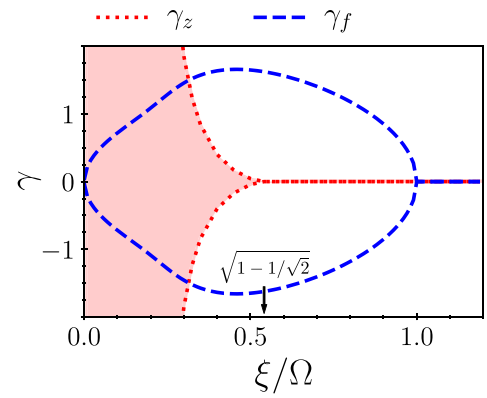

FIG. 5. Phase diagram in γ-ξ plane at $E_\phi = 0$. γ_z separates the shaded region with three zeros of σ from the rest with one zero. γ_f is the boundary where the profiles of σ flips at one peak. At $\xi/\Omega \geqslant 1$, we are in the weak-coupling regime where $\gamma_z, \gamma_f = 0$, and σ always has a single zero when the peak and dip exchange position as we move around $\gamma = 0$.

E. Finite detuning from the center of V_E: $E_\phi \neq 0$

We take the location of the maximum of the interaction V_E at $E = 0$, so E_ϕ measures its detuning from the discrete state. We know that the Fano resonance simply shifts with E_ϕ in the weak-coupling regime. We find that, in the strong-coupling regime, the effect of $E_\phi \neq 0$ at small values is, roughly speaking, to cooperate or compete γ, depending on the relative sign of E_ϕ and γ. Figure 6 shows σ at $\xi/\Omega = 0.3$ at three values of $E_\phi/\Omega = -0.5, 0, 0.5$ (rows), and three values of $\gamma = 0, 1, 5$ (columns). The effect of γ on σ at $E_\phi = 0$ is discussed in Sec. IV C. Here the middle row, Figs. 6(d)–6(f), shows the same again. We see that at negative E_ϕ, Figs. 6(a)–6(c), the effect of γ is enhanced, while at positive E_ϕ, Figs. 6(g)–6(i), it is compensated by a finite E_ϕ. At negative γ (not shown), the profile would be mirrored around $E = 0$ and the role of $\pm E_\phi$ would be swapped.

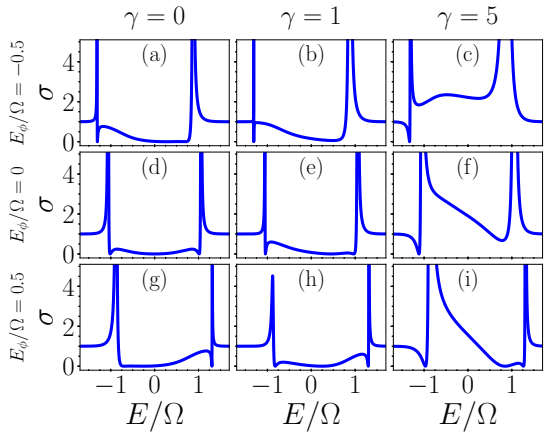

FIG. 6. Effect of detuning $E_\phi \neq 0$ in the strong-coupling regime. σ at $\xi/\Omega = 0.3$ at $E_\phi/\Omega = -0.5, 0, 0.5$ (rows), and $\gamma = 0, 1, 5$ (columns). We see that $E_\phi < 0$ cooperates with γ and enhances its effect [compare (d) and (e) with (a)–(c)] while $E_\phi > 0$ competes with it and suppresses its effect [compare (d) and (e) with (g) and (h)].

F. Discrete state outside the continuum

The Fano resonance in the weak-coupling regime requires the discrete state to lie within the continuum. We find that if the coupling is strong enough, σ can still obtain its characteristic features around the center of V_E, even if the discrete state lies well outside the continuum. This is plausible as a large detuning would reduce the effective coupling between the discrete state and the continuum and thus could lead to the results similar to the weak-coupling regime. In our calculations, at $E_\phi \gg \xi$, we do not actually need to limit the bandwidth of the continuum to push the discrete state outside. Instead, we can focus on the continuum states around $E = 0$ that are coupled to the discrete state and ignore the continuum states well outside the interaction range (a few ξ) that are practically uncoupled from the discrete state.

Figure 7 shows σ at $\xi/\Omega = 0.3$, $E_\phi/\Omega = 5.0$ and four values of γ chosen to present four characteristic profiles that

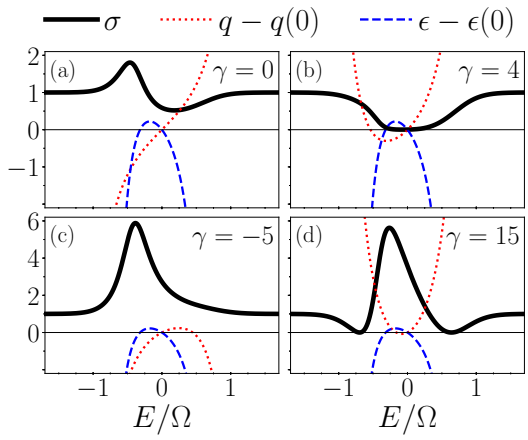

FIG. 7. A discrete state *outsite* the continuum in the strong-coupling regime. q, ϵ, σ are shown at $\xi/\Omega = 0.3$, $E_\phi/\Omega = 5.0$, and $\gamma = -5, 0, 4, 15$. σ exhibits features similar to the weak-coupling regime (a)–(c) and (d) a new profile with two zeros around a peak.

can be obtained in such a case. It also shows corresponding q and ϵ (shifted by their values at $E = 0$) to show the origin of these profiles. We see that σ in Figs. 7(a)–7(c), resembles the characteristic weak-coupling cases corresponding to the constant asymmetry parameter $q = -1, 0, \infty$. In addition, Fig. 7(d) shows a profile with two zeros around a peak that does not exist in the weak-coupling case.

We can understand this behavior by noting that at large $E_\phi \gg \Omega$, the discrete state and the continuum states within the interaction peak will slightly perturb each other, exchanging a tiny bit of their spectral weights (transferring it to the eigenstates at their locations). This will create a small peak in the spectral component c_ϕ of $|\phi\rangle$ around $E = 0$ and a corresponding small dip in the spectral components c_ψ of the "local" continuum states $|\psi_E\rangle$, which is 1 everywhere around $E = 0$ but at this dip. The interference between the transition amplitudes from these spectral components is controlled by γ and, at $|\gamma| \gg 1$ [Figs. 7(b)–7(d)] where we can ignore the "nonlocal" continuum dragged along with c_ϕ, we have $\sigma \simeq (\gamma c_\phi - c_\psi)^2$. At $\gamma = -5$ [Fig. 7(c)], γc_ϕ becomes a dip and *adds up* to the dip in c_ψ, creating a large peak in σ. At positive γ, the peak of γc_ϕ increases with an increase in γ and at some point meets it, creating a dip structure [Fig. 7(b)]. At larger γ, the peak of γc_ϕ crosses the dip of c_ψ making $\sigma \to 0$ at *two* locations where the two amplitudes cancel each other completely [Fig. 7(d)]. The dip and peak structure in Fig. 7(a) seen at $\gamma = 0$ is caused by the interference between the local continuum states and the nonlocal continuum states pulled along by $|\phi\rangle$ (the $|\psi_E\rangle$ components of $|\Phi\rangle$), instead of $|\phi\rangle$ itself.

We find that, for $E_\phi \to -E_\phi$ and $\gamma \to -\gamma$, $\sigma(E) \to \sigma(-E)$, so had we used $E_\phi/\Omega = -5.0$, we would have obtained $q = +1$ profile at $\gamma = 0$ instead of Fig. 7(a).

V. A HOMOGENEOUSLY BROADENED STATE INSTEAD OF A CONTINUUM

A localized interaction with a continuum can also arise in case of various open quantum systems, e.g., plasmonic and photonic nanostructures that host broad resonances, which can couple to relatively narrow electronic, vibrational, or other states. Such broadened states are known only through their density of states or spectral function.

To calculate the scattering from a broadened state that is coupled to a localized discrete state, Giannini *et al.* introduced a method in Ref. [18] that treats the broadened state like a continuum of states but with its interaction with the narrow state and its bare transition matrix element proportional to the square root of its spectral function. Here we provide an alternative approach to treat the same problem that is not only physically motivated but mathematically more rigorous as well. Besides, it gives a deeper insight into the behavior of the system and can also be generalized to treat interaction between multiple broadened states to study their weak- and strong-coupling regimes, for instance.

Our approach is simple. We enlarge the Hilbert space to include the environment in the model and work with the underlying eigenstates that produce the desired spectral distribution of the broadened state. Let us suppose $\mathcal{A}_{E,\bar{\phi}}$ is the spectral function of a broadened state. If the broadening is

Lorentzian centered around an energy $E_{\bar{\phi}}$, then

$$\mathcal{A}_{E,\bar{\phi}} = \frac{1}{\pi}\frac{\Gamma_{\bar{\phi}}/2}{(E-E_{\bar{\phi}})^2+\Gamma_{\bar{\phi}}^2/4}, \tag{34}$$

where $\Gamma_{\bar{\phi}}$ is the width of the distribution. We can consider a *constant* coupling $\bar{V}_E = \sqrt{\Gamma_{\bar{\phi}}/2\pi}$ (the subscript E is used for consistency) between the parent discrete state $|\bar{\phi}\rangle$ and the continuum of its environment states $|\bar{\psi}_E\rangle$, which form a continuum of eigenstates $|\psi_E\rangle$ that describe the spectral function $\mathcal{A}_{E,\bar{\phi}}$ correctly (self-consistently). Now, to describe the interaction of the broadened state with a discrete state, $|\psi_E\rangle$ can be coupled to it instead.

Assuming we have a discrete state $|\phi\rangle$ at energy E_ϕ with a coupling λ to the state $|\bar{\phi}\rangle$, we can compute the corresponding coupling V_E between $|\phi\rangle$ and $|\psi_E\rangle$ and calculate the eigenstates of the full (closed quantum) system $|\Psi_E\rangle$. Following this procedure (see Appendix A 2), and expressing $|\Psi_E\rangle$ in terms of the bare states of the system and the environment, we obtain

$$\begin{aligned}
|\Psi_E\rangle &= c_{E,\phi}\,|\phi\rangle + c_{E,\bar{\phi}}\,|\bar{\phi}\rangle + \fint dE' c_{E,\bar{\psi}_{E'}}\,|\bar{\psi}_{E'}\rangle,\\
c_{E,\phi} &= \frac{\sin\Delta_E}{\pi V_E},\\
c_{E,\bar{\phi}} &= \frac{\sin\Delta_E}{\pi V_E}\frac{F_E}{\lambda} - \cos\Delta_E\frac{V_E}{\lambda},\\
c_{E,\bar{\psi}_{E'}} &= \frac{\sin\Delta_E}{\pi V_E}\left(\frac{\bar{V}_{E'}G_{E,E'}}{\lambda} - \frac{V_{E'}\cos\bar{\Delta}_{E'}}{E-E'}\right)\\
&\quad - \frac{V_E\cos\Delta_E\bar{V}_{E'}}{\lambda(E-E')} + \cos\Delta_E\cos\bar{\Delta}_E\delta(E-E'),
\end{aligned} \tag{35}$$

where

$$\begin{aligned}
G_{E,E'} &= \fint dE''\frac{V_{E''}^2}{(E-E'')(E''-E')},\\
\bar{\Delta}_E &= -\arctan[\pi\bar{V}_E^2/(E-E_{\bar{\phi}})],\\
\Delta_E &= -\arctan[\pi V_E^2/(E-E_\phi-F_E)],\\
V_E &= \lambda\frac{\sin\bar{\Delta}_E}{\pi\bar{V}_E},\\
F_E &= \lambda^2\frac{E-E_{\bar{\phi}}}{(E-E_{\bar{\phi}})^2+\Gamma_{\bar{\phi}}^2/4}.
\end{aligned} \tag{36}$$

We can now write the scattering amplitude $\mathcal{M}_E = \langle i|\hat{T}|\Psi_E\rangle$ in terms of the scattering amplitudes $\mathcal{M}_\phi = \langle i|\hat{T}|\phi\rangle$ and $\mathcal{M}_{\bar{\phi}} = \langle i|\hat{T}|\bar{\phi}\rangle$ of the bare states $|\phi\rangle$ and $|\bar{\phi}\rangle$, and that of the environment $\mathcal{M}_{\bar{\psi}_{E'}} = \langle i|\hat{T}|\bar{\psi}_{E'}\rangle$, as

$$\mathcal{M}_E = c_{E,\phi}\mathcal{M}_\phi + c_{E,\bar{\phi}}\mathcal{M}_{\bar{\phi}} + \fint dE' c_{E,\bar{\psi}_{E'}}\mathcal{M}_{\bar{\psi}_{E'}}. \tag{37}$$

Assuming that $\mathcal{M}_{\bar{\psi}_{E'}}$ vanishes identically for the considered scattering process, and $\mathcal{M}_\phi$, $\mathcal{M}_{\bar{\phi}}$ are real, the scattering probability $|\mathcal{M}_E|^2$ can be simplified to obtain

$$|\mathcal{M}_E|^2 = \frac{(E\mathcal{M}_{\bar{\phi}} + \lambda\mathcal{M}_\phi)^2\mathcal{A}_{E,\bar{\phi}}}{E^2 + \left[\lambda^2 - 2E(E-E_{\bar{\phi}})\right]\frac{2\pi\lambda^2}{\Gamma_{\bar{\phi}}}\mathcal{A}_{E,\bar{\phi}}}, \tag{38}$$

where $E_\phi = 0$ is taken as reference. It can be cast into the form obtained by Giannini *et al.* [18] by normalizing it with $\mathcal{A}_{E,\bar{\phi}}\mathcal{M}_{\bar{\phi}}^2$ (see Appendix A 2).

As discussed in the Introduction, this model also exhibits the strong-coupling regime, where the "secular equation" $E - E_{\bar{\phi}} - F_E = 0$ admits multiple solutions, indicating the emergence of new hybrid states that split off the two bare states, similarly to the appearance of lower and upper polaritons in microcavities, for instance. We find that the strong-coupling regime occurs at $\lambda > \Gamma_{\bar{\phi}}/2$ in this case, which agrees to the typical criterion in microcavities assuming only one of the emitter and cavity states is broadened or lossy. The method can be generalized to treat multiple broadened states by including their environment(s) in the picture.

Apart from the obvious application to study various scattering spectra of systems involving broadened states similar to Ref. [18], the fact that this method can use the concepts and tools of closed quantum systems makes it much more powerful. For example, the eigenstates $|\Psi_E\rangle$ of the "system+environment" can be used to study the transition between weak- and strong-coupling regimes of the system, the exact non-Markovian dynamics of the system in either of the phases, and the redistribution of the spectral weights of the broadened states as in spectral hole burning [48].

VI. SUMMARY AND DISCUSSION

We showed that the Fano's model with a strongly localized interaction can appear in important physical systems involving a genuine continuum of states. Using a Gaussian interaction profile, we showed that the model exhibits a strong-coupling phase for the Gaussian width ξ (standard deviation) below the collective coupling Ω. We find that new resonances with ultra sharp features appear in the strong-coupling phase where the scattering probability for a generic scattering process can exhibit complete destructive interference at one or three positions, depending on the ratio of its bare transition amplitudes γ. We calculated the phase diagram of the model in the space of its two parameters γ, ξ and find that above a critical value $\xi/\Omega = \sqrt{1-1/\sqrt{2}}$, complete destructive interference can occur once at most. We also find that a discrete state far detuned from the center of the interaction or even outside the continuum can produce some features of the weak-coupling Fano resonances if its collective coupling is strong enough.

We also considered systems involving a broadened state instead of a continuum of states and present a method to treat such problems. We explicitly consider the continuum states of the environment that induces the broadening and show that it is possible to calculate the eigenstates of the resulting closed quantum system. The application of this method is not limited to calculating the scattering probability, however. The eigenstates can be used to *exactly* calculate the static and dynamic properties of the system without any approximations on the correlations between the system and its environment, which is typically intractable.

In addition to the disordered Tavis-Cummings model, another interesting cavity QED system where a continuum of states collectively couple to a discrete state with a localized interaction is a single emitter coupled to a cavity if the cavity

confines the electromagnetic field in less than all three spatial dimensions, e.g., a planner microcavity. In such cases, the cavity modes at a continuum of the in-plane wave vectors $k_\parallel$ exist, which form the cavity band that couples to the discrete emitter state. Since the electric dipole interaction depends on the relative orientation of the emitters' transition dipole moment $\vec{d}$ and the electric field $\vec{E}$, the interaction contains a factor of $\cos\theta$, where θ is the angle between $\vec{E}$ and $\vec{d}$, which will be a function of $k_\parallel$ for a fixed emitter. The interaction $V_E \propto \cos^2\theta$ will then be localized around $\theta = 0$ that maps to a localization in $k_\parallel$ and hence energy of the band. In the single excitation space, this becomes Fano's model and the results presented in this article and in Ref. [28] would be relevant to it as well. Since the role of the cavity and emitter states is exchanged in this case as compared to energetically disordered TC model studied in Ref. [28], $\gamma = 0$ for the the optical spectrum here so we should observe complete destructive interference in it at one or three energies as in Figs. 4(e) and 4(m). Furthermore, as the exact eigenstates of the model can be computed, we can also study an effective coupling between the continuum of cavity states induced by their collective coupling to the emitter, which would be similar to an effective coupling induced between multiple emitters when they collectively couple to a common cavity mode.

The phase diagram at $E_\phi = 0$ that is presented in this work is only a slice in the full γ, ξ, E_ϕ space. It would certainly be interesting to explore how it evolves with $E_\phi = 0$ to completely characterize the model. An experimental study to verify our results and finding other realizations of the model with a localized interaction can also be interesting future works.

Fortunately, the approach to treat a broadened state presented here is also tractable for multiple broadened states interacting with each other, whether the broadening is caused by a single common environment or different individual environments. Systems where narrow and broad states interact, e.g., plasmonic nanostructures, can thus be treated with this method taking into account the broadening of all states involved. This observation also creates a temptation to apply it to paradigmatic models of cavity QED, e.g., Jaynes-Cummings model, to treat the cavity and emitter losses "exactly" to investigate their effects on the eigenstates and the weak- to strong-coupling transition. Our preliminary calculations show that some interesting aspects of the nature of the polariton states in such lossy systems can be revealed with this method. For instance, the exact relation between the linewidths of the polariton states and the linewidths of its parent states can be explored. Questions like these can be addressed in a future study.

ACKNOWLEDGMENT

The author thanks Rukhshanda Naheed for fruitful discussions.

APPENDIX

1. A single zero of σ at $\xi/\Omega \geqslant \sqrt{1-1/\sqrt{2}}$

Setting $\gamma = 0$ in Eq. (29) and using it with Eq. (23), we can expand $q + \epsilon = 0$ at small E to obtain

$$\mathrm{erfi}(E/2\xi) + \sqrt{\frac{2}{\pi}}\frac{\xi}{\Omega^2} e^{E^2/2\xi^2} E - \mathrm{erfi}(E/\sqrt{2}\xi) = 0, \quad \text{(A1)}$$

$$[\sqrt{2} + 2(\xi/\Omega)^2 - 2 + (E/\Omega)^2]E = 0. \quad \text{(A2)}$$

Considering the root $E \neq 0$, the term in the brackets gives $\xi/\Omega = \sqrt{1 - 1/\sqrt{2} - (E/\Omega)^2/2}$, which approaches $\xi/\Omega = \sqrt{1-1/\sqrt{2}} \simeq 0.54$ as this root E approaches $E = 0$.

2. Interaction between a discrete state and a broadened state: Calculation of the eigenstates

Considering a coupling $\bar{V}_E = \sqrt{\Gamma_{\bar{\phi}}/2\pi}$ between $|\bar{\phi}\rangle$ and $|\bar{\psi}_E\rangle$, their continuum of eigenstates $|\psi_E\rangle$ have the same structure as Eq. (11) and are given by

$$|\psi_E\rangle = \frac{\sin\bar{\Delta}_E}{\pi\bar{V}_E}\left(|\bar{\phi}\rangle + \int \frac{\bar{V}_{E'}}{E-E'} dE' \, |\bar{\psi}_{E'}\rangle\right) - \cos\bar{\Delta}_E \, |\bar{\psi}_E\rangle, \quad \text{(A3)}$$

where $\bar{\Delta}_E = -\arctan[\pi\bar{V}_E^2/(E - E_{\bar{\phi}})]$.

The spectral function of the state $|\bar{\phi}\rangle$ is given by the square of its coefficient in $|\psi_E\rangle$, i.e., $\mathcal{A}_{E,\bar{\phi}} = \sin^2\bar{\Delta}_E/\pi^2\bar{V}_E^2$, and we can easily see that it agrees to Eq. (34), showing the desired consistency between $\bar{V}_E$ and $\mathcal{A}_{E,\bar{\phi}}$.

We can now couple $|\psi_E\rangle$ to the state $|\phi\rangle$ at energy E_ϕ. If λ is the coupling between $|\phi\rangle$ and $|\bar{\phi}\rangle$, the coupling V_E between $|\phi\rangle$ and $|\psi_E\rangle$ becomes $V_E = \lambda \sin\bar{\Delta}_E/\pi\bar{V}_E$, which is equal to $\lambda\sqrt{\mathcal{A}_{E,\bar{\phi}}}\mathrm{sign}(E_{\bar{\phi}} - E)$—similarly to Ref. [18] except for a possibly negative sign at $E > E_{\bar{\phi}}$. The eigenstates of the full (closed quantum) system $|\Psi_E\rangle$ can now be easily written down in an analogy to Eq. (11) again, given by

$$|\Psi_E\rangle = \frac{\sin\Delta_E}{\pi V_E}\left(|\phi\rangle + \int \frac{V_{E'}}{E-E'} dE' \, |\psi_{E'}\rangle\right) - \cos\Delta_E \, |\psi_E\rangle, \quad \text{(A4)}$$

where Δ_E is given in Eq. (36). $|\psi_E\rangle$ in Eq. (A3) can now be substituted into Eq. (A4) to obtain Eq. (35) in the main text.

The final expression for the scattering probability that is given in Eq. (38) in the main text can be compared with Eq. (6) in Ref. [18] using the following correspondence: $(\lambda, E_\phi, E_{\bar{\phi}}, \Gamma_{\bar{\phi}}) \leftrightarrow (v, E_d, E_p, \Gamma_p)$, $(\mathcal{M}_\phi, \mathcal{M}_{\bar{\phi}}, \mathcal{M}_E) \leftrightarrow (w, c, \langle i|W|\Psi\rangle)$, and $\mathcal{A}_{E,\bar{\phi}} \leftrightarrow \frac{2}{\pi\Gamma_p}\mathcal{L}(E)$ ($\mathcal{L}(E)$ is unnormalized).

[1] U. Fano, Phys. Rev. **124**, 1866 (1961).
[2] W. Zhang, A. O. Govorov, and G. W. Bryant, Phys. Rev. Lett. **97**, 146804 (2006).
[3] S. Zhang, D. A. Genov, Y. Wang, M. Liu, and X. Zhang, Phys. Rev. Lett. **101**, 047401 (2008).
[4] T.-T. Tang, Y. Zhang, C.-H. Park, B. Geng, C. Girit, Z. Hao, M. C. Martin, A. Zettl, M. F. Crommie, S. G. Louie, Y. R. Shen, and F. Wang, Nat. Nanotechnol. **5**, 32 (2010).
[5] C. Ott, A. Kaldun, P. Raith, K. Meyer, M. Laux, J. Evers, C. H. Keitel, C. H. Greene, and T. Pfeifer, Science **340**, 716 (2013).

[6] H. G. Luo, T. Xiang, X. Q. Wang, Z. B. Su, and L. Yu, Phys. Rev. Lett. **92**, 256602 (2004).

[7] A. Zielinski, V. P. Majety, S. Nagele, R. Pazourek, J. Burgdörfer, and A. Scrinzi, Phys. Rev. Lett. **115**, 243001 (2015).

[8] Y. Wang, L. Liao, T. Hu, S. Luo, L. Wu, J. Wang, Z. Zhang, W. Xie, L. Sun, A. V. Kavokin, X. Shen, and Z. Chen, Phys. Rev. Lett. **118**, 063602 (2017).

[9] H. Beutler, Z. Phys. **93**, 177 (1935).

[10] U. Fano, Il Nuovo Cimento (1924-1942) **12**, 154 (1935).

[11] M. Kroner, A. O. Govorov, S. Remi, B. Biedermann, S. Seidl, A. Badolato, P. M. Petroff, W. Zhang, R. Barbour, B. D. Gerardot, R. J. Warburton, and K. Karrai, Nature (Lond.) **451**, 311 (2008).

[12] C. P. Holfeld, F. Löser, M. Sudzius, K. Leo, D. M. Whittaker, and K. Köhler, Phys. Rev. Lett. **81**, 874 (1998).

[13] S. Flach, A. E. Miroshnichenko, V. Fleurov, and M. V. Fistul, Phys. Rev. Lett. **90**, 084101 (2003).

[14] S. Flach, V. Fleurov, A. V. Gorbach, and A. E. Miroshnichenko, Phys. Rev. Lett. **95**, 023901 (2005).

[15] P. Binder, D. Abraimov, A. V. Ustinov, S. Flach, and Y. Zolotaryuk, Phys. Rev. Lett. **84**, 745 (2000).

[16] E. Trías, J. J. Mazo, and T. P. Orlando, Phys. Rev. Lett. **84**, 741 (2000).

[17] M. Galli, S. L. Portalupi, M. Belotti, L. C. Andreani, L. O'Faolain, and T. F. Krauss, Appl. Phys. Lett. **94**, 071101 (2009).

[18] V. Giannini, Y. Francescato, H. Amrania, C. C. Phillips, and S. A. Maier, Nano Lett. **11**, 2835 (2011).

[19] Y. Francescato, V. Giannini, and S. A. Maier, ACS Nano **6**, 1830 (2012).

[20] K.-L. Lee, H.-Y. Hsu, M.-L. You, C.-C. Chang, M.-Y. Pan, X. Shi, K. Ueno, H. Misawa, and P.-K. Wei, Sci. Rep. **7**, 44104 (2017).

[21] J. Göres, D. Goldhaber-Gordon, S. Heemeyer, M. A. Kastner, H. Shtrikman, D. Mahalu, and U. Meirav, Phys. Rev. B **62**, 2188 (2000).

[22] K. Kobayashi, H. Aikawa, S. Katsumoto, and Y. Iye, Phys. Rev. Lett. **88**, 256806 (2002).

[23] A. C. Johnson, C. M. Marcus, M. P. Hanson, and A. C. Gossard, Phys. Rev. Lett. **93**, 106803 (2004).

[24] A. E. Miroshnichenko, S. Flach, and Y. S. Kivshar, Rev. Mod. Phys. **82**, 2257 (2010).

[25] B. Luk'yanchuk, N. I. Zheludev, S. A. Maier, N. J. Halas, P. Nordlander, H. Giessen, and C. T. Chong, Nat. Mater. **9**, 707 (2010).

[26] M. F. Limonov, M. V. Rybin, A. N. Poddubny, and Y. S. Kivshar, Nat. Photon. **11**, 543 (2017).

[27] D. G. Lidzey, D. Bradley, M. Skolnick, T. Virgili, S. Walker, and D. Whittaker, Nature (Lond.) **395**, 53 (1998).

[28] M. A. Zeb, Analytical solution of the disordered Tavis-Cummings model and its fano resonances, arXiv:2208.11990 (2022).

[29] E. J. Osley, C. G. Biris, P. G. Thompson, R. R. F. Jahromi, P. A. Warburton, and N. C. Panoiu, Phys. Rev. Lett. **110**, 087402 (2013).

[30] M. Tavis and F. W. Cummings, Phys. Rev. **170**, 379 (1968).

[31] M. Tavis and F. W. Cummings, Phys. Rev. **188**, 692 (1969).

[32] J. Kasprzak, M. Richard, S. Kundermann, A. Baas, P. Jeambrun, J. M. J. Keeling, F. M. Marchetti, M. H. Szymańska, R. André, J. L. Staehli, V. Savona, P. B. Littlewood, B. Deveaud, and L. S. Dang, Nature (Lond.) **443**, 409 (2006).

[33] A. A. Houck, H. E. Türeci, and J. Koch, Nat. Phys. **8**, 292 (2012).

[34] J. Keeling and S. Kéna-Cohen, Annu. Rev. Phys. Chem. **71**, 435 (2020).

[35] V. Kravtsov, E. Khestanova, F. A. Benimetskiy, T. Ivanova, A. K. Samusev, I. S. Sinev, D. Pidgayko, A. M. Mozharov, I. S. Mukhin, M. S. Lozhkin, Y. V. Kapitonov, A. S. Brichkin, V. D. Kulakovskii, I. A. Shelykh, A. I. Tartakovskii, P. M. Walker, M. S. Skolnick, D. N. Krizhanovskii, and I. V. Iorsh, Light Sci. Appl. **9**, 56 (2020).

[36] F. I. Moxley, E. O. Ilo-Okeke, S. Mudaliar, and T. Byrnes, Emerg. Mater. **4**, 971 (2021).

[37] P. Berini and I. De Leon, Nat. Photon. **6**, 16 (2012).

[38] M. T. Hill and M. C. Gather, Nat. Photon. **8**, 908 (2014).

[39] D. Sanvitto and S. Kéna-Cohen, Nat. Mater. **15**, 1061 (2016).

[40] T. Low, A. Chaves, J. D. Caldwell, A. Kumar, N. X. Fang, P. Avouris, T. F. Heinz, F. Guinea, L. Martin-Moreno, and F. Koppens, Nat. Mater. **16**, 182 (2017).

[41] C. Schneider, M. M. Glazov, T. Korn, S. Höfling, and B. Urbaszek, Nat. Commun. **9**, 2695 (2018).

[42] R. Su, A. Fieramosca, Q. Zhang, H. S. Nguyen, E. Deleporte, Z. Chen, D. Sanvitto, T. C. H. Liew, and Q. Xiong, Nat. Mater. **20**, 1315 (2021).

[43] Q. Zhang, G. Hu, W. Ma, P. Li, A. Krasnok, R. Hillenbrand, A. Alù, and C.-W. Qiu, Nature (Lond.) **597**, 187 (2021).

[44] R. Houdré, R. P. Stanley, and M. Ilegems, Phys. Rev. A **53**, 2711 (1996).

[45] J. Mony, C. Climent, A. U. Petersen, K. Moth-Poulsen, J. Feist, and K. Börjesson, Adv. Funct. Mater. **31**, 2010737 (2021).

[46] T. Gera and K. L. Sebastian, J. Chem. Phys. **156**, 194304 (2022).

[47] R. F. Ribeiro, L. A. Martínez-Martínez, M. Du, J. Campos-Gonzalez-Angulo, and J. Yuen-Zhou, Chem. Sci. **9**, 6325 (2018).

[48] W.-J. Zhou, J.-b. You, X. Xiong, Y.-W. Lu, L. K. Ang, J.-F. Liu, and L. Wu, Nanotechnology **33**, 475001 (2022).